nature chemistry

Article

https://doi.org/10.1038/s41557-024-01564-3

Establishing the origin of Marcus-inverted-region behaviour in the excited-state dynamics of cobalt(III) polypyridyl complexes

Received: 18 September 2023

Accepted: 24 May 2024

Published online: 04 July 2024

Check for updates

Atanu Ghosh, Jonathan T. Yarranton & James K. McCusker

Growing interest in the use of first-row transition metal complexes in a number of applied contexts—including but not limited to photoredox catalysis and solar energy conversion—underscores the need for a detailed understanding of their photophysical properties. A recent focus on ligand-field photocatalysis using cobalt(III) polypyridyls in particular has unlocked unprecedented excited-state reactivities. Photophysical studies on Co(III) chromophores in general are relatively uncommon, and so here we carry out a systematic study of a series of Co(III) polypyridyl complexes in order to delineate their excited-state dynamics. Compounds with varying ligand-field strengths were prepared and studied using variable-temperature ultrafast transient absorption spectroscopy. Analysis of the data establishes that the ground-state recovery dynamics are operating in the Marcus inverted region, in stark contrast to what is typically observed in other first-row metal complexes. The analysis has further revealed the underlying reasons driving this excited-state behaviour, thereby enabling potential advancements in the targeted use of the Marcus inverted region for a variety of photolytic applications.

The photophysical properties of transition metal-based complexes have been studied extensively for decades due in part to their pivotal role in light-enabled chemical processes ranging from solar energy conversion strategies to photoredox catalysis[1–6]. Despite this success, recently considerable attention has been placed on sustainability and scalability for chemical transformations; in transition metal chemistry, this largely requires a shift in focus to the more abundant and cheaper elements of the first transition series[7–11]. While this has resulted in exciting and potentially transformative developments in areas such as catalysis[6], the replacement of chromophores based on Ru and Ir (for example, with first-row analogues to effect analogous excited-state chemistry) has proven to be considerably more challenging.

The primary difficulty stems from fundamental differences in electronic structure that impact non-radiative decay dynamics due to the presence of lower-lying ligand-field states (that is, '*d*–*d*' states)[7,12–17]. These metal-centred excited states are characterized by a rearrangement of electrons within the *d*-orbital manifold as opposed to a formal separation of charge, which substancially changes the landscape in terms of the type of excited-state chemistry that can be anticipated. Indeed, with a number of notable exceptions involving Cr(III) (ref. 18), chemical platforms have been only recently developed that are providing promise along these lines[19].

Among the other first-row transition metal complexes, low-spin d^6-Fe(II) complexes have garnered considerable attention. For Fe(II) polypyridyl complexes (for example, $[Fe(bpy)_3]^{2+}$, where bpy is 2,2'-bipyridine), the initially formed metal-to-ligand charge-transfer (MLCT) excited state decays on a sub-100 fs timescale to the ligand-field manifold, ultimately forming a high-spin $S = 2$ species

Department of Chemistry, Michigan State University, East Lansing, MI, USA. e-mail: jkm@chemistry.msu.edu

https://doi.org/10.1038/s41557-024-01564-3

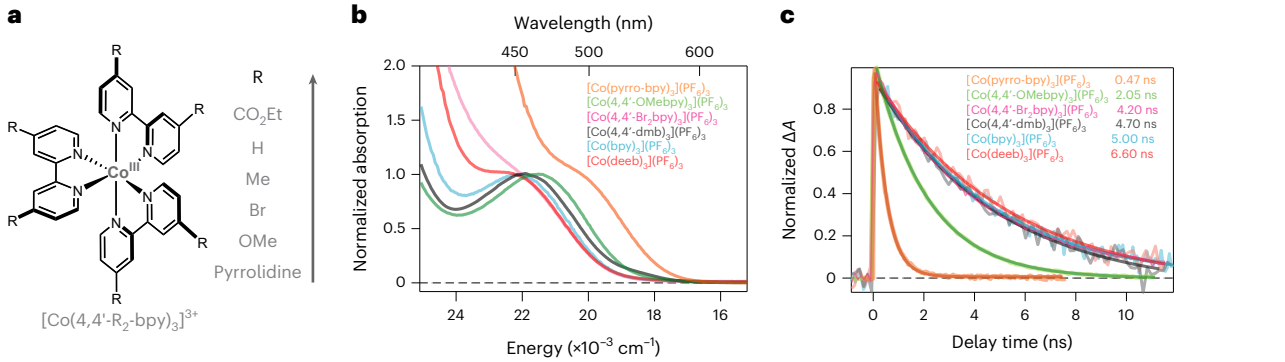

Fig. 1 | Structure, ground-state and excited-state properties. a, Drawing of the six Co(III) polypyridyl complexes examined in this study. All compounds were of the general form $[Co(4,4'\text{-}R_2\text{-}bpy)_3](PF_6)_3$ and are characterized by increasing ligand-field strength as indicated by the arrow. **b**, Normalized electronic absorption spectra of all six complexes collected in acetonitrile solution, revealing a blueshift in the $^1A_1 \rightarrow {}^1T_1$ absorption maximum with increasing ligand-field strength. **c**, Transient absorption kinetics of all six complexes shown in **a**, acquired in acetonitrile solution at room temperature subsequent to $^1A_1 \rightarrow {}^1T_1$ photoexcitation. The lifetimes shown in the inset derive from fits to single-exponential kinetic models and are also tabulated in Supplementary Table 1.

(the $^5T_2$ ligand-field state)[20]. While such ligand-field excited states have been shown to engage in bimolecular electron-transfer chemistry[21], the relatively low energy coupled with an ~1 ns lifetime limits the utility of such compounds for bimolecular photochemical transformations in particular. Several approaches have emerged to alter the excited-state energetic profile of these complexes[22–28], but such efforts are hampered by the inability to assess the energies of ligand-field states in chromophores whose absorption spectra are dominated by much more intense MLCT features in the visible region[21]. In the case of Fe(II) complexes, we have shown that this problem can be circumvented by using isoelectronic low-spin d^6-Co(III) complexes[29]. The ligand-to-metal charge-transfer (LMCT) absorptions characteristic of Co(III) complexes are dramatically blueshifted relative to their MLCT counterparts in Fe(II), thereby revealing the previously obscured ligand-field absorption features associated with the d^6 configuration. Observations of spin-allowed ($^1A_1 \rightarrow {}^1T_1$) and spin-forbidden ($^1A_1 \rightarrow {}^3T_1$, $^1A_1 \rightarrow {}^3T_2$) transitions were successfully leveraged to explicitly determine the relevant ligand-field parameters of a series of Co(III) compounds.

Having such quantitative information concerning the ligand-field excited states of these compounds—and given recent examples of Co(III)-based complexes as photocatalysts[30–35]—we wanted to probe the photo-induced dynamics of these compounds. A surprisingly small number of ultrafast photophysical studies of Co(III) complexes exist[36–43]. Recently, we reported excited-state lifetimes of a family of tris-bipyridyl-based Co(III) complexes[35] where a striking correlation between increasing excited-state lifetime with increasing ligand-field strength was observed, a phenomenology consistent with dynamics occurring in the Marcus inverted region. However, these room temperature kinetic data alone are not conclusive for establishing inverted-region behaviour, nor do they provide insight as to its origins. We therefore carried out a thorough photophysical study on a series of Co(III) complexes using variable-temperature transient absorption spectroscopy. Analysis of these data using several non-radiative decay theories—most notably semi-classical Marcus theory—provide vital insights into the nature of the lowest-energy excited states of these compounds, insights that allow us to draw definitive conclusions concerning the inverted-region hypothesis. Furthermore, the results allowed us to identify the reason why inverted behaviour is observed for this class of compounds as opposed to the normal region dynamics seen for isoelectronic Fe(II) complexes. We believe these results open the door to exploiting this phenomenon in a broader range of applications involving light-to-chemical energy conversion strategies.

Results and discussion

The structures of tris-bipyridyl Co(III) complexes studied here are shown in Fig. 1a. All compounds possess low-spin, d^6 configurations[29] and their visible absorption spectra are plotted in Fig. 1b. The systematic shift in the absorption maximum reflects an increase in the ligand-field strength across the series, with values of 10Dq, the ligand-field splitting parameter, ranging from 22,440 cm^{-1} in the case of $[Co(pyrro\text{-}bpy)_3](PF_6)_3$ to 24,620 cm^{-1} for $[Co(deeb)_3](PF_6)_3$ (where pyrro-bpy and deeb are 4,4′-di-pyrrolodine-2,2′-bipyridine and 4,4′-di-ethylcarboxylate-2,2′-bipyridine, respectively; Supplementary Table 1).

Transient absorption spectroscopy

The absence of overlapping charge-transfer features in the visible region of these Co(III) complexes allows for direct excitation into the $^1A_1 \rightarrow {}^1T_1$ transition: we therefore bypass the charge-transfer manifold entirely, allowing us to focus exclusively on dynamics occurring within the metal-centred ligand-field manifold of the compounds. As an initial probe, we carried out ultrafast time-resolved absorption measurements at room temperature on all six complexes to assess the overall timescale of their ground-state recovery dynamics. The data, which we reported recently[35] but have replotted in Fig. 1c for convenience, recover fully to the baseline and therefore represent a completely reversible photophysical process.

The trend in excited-state lifetime (Supplementary Table 1) varies systematically, suggesting a clear correlation between the observed excited-state lifetime and the magnitude of 10Dq. Specifically, the data reveal that an inverse relationship exists between the magnitude of 10Dq and the rate constant for ground-state recovery: as 10Dq increases, the rate constant for excited-state relaxation back to the ground state decreases. While this type of behaviour is commonly observed for complexes such as ruthenium(II) polypyridyls (for example, $[Ru(bpy)_3]^{2+}$), where relaxation of the lowest-energy ^{3}MLCT excited state follows the so-called energy gap law[44], this was a wholly unexpected result for these d^6-Co(III) complexes due to the interconfigurational nature of all of the ligand-field excited states for a d^6 configuration.

To appreciate this latter point, recall that the energy gap law is based on straightforward arguments stemming from non-radiative decay theory as depicted schematically in Fig. 2 (ref. 45). When the zero-point energy difference between the ground state and lowest-energy excited state is larger than the energy, reflecting structural differences between their equilibrium geometries (Fig. 2a), non-radiative decay theory predicts a decrease in the rate constant for conversion from the upper state to the lower state with an increasing energy gap due to the decrease in the overlap between the ground

https://doi.org/10.1038/s41557-024-01564-3

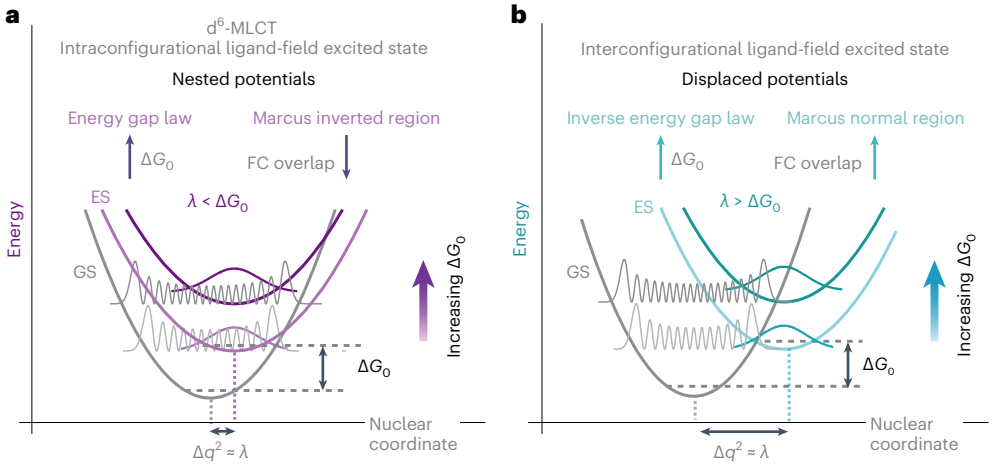

Fig. 2 | Schematic representation of the energy gap law and Marcus theory. **a**, Minimal structural differences (Δq) between the equilibrium exited-state (ES) and ground-state (GS) geometries give rise to nested potentials. The decrease in Franck–Condon (FC) overlap, with the increasing zero-point energy difference this situation creates, leads to a decrease in the rate constant for non-radiative decay back to the ground state, resulting in an increase in excited-state lifetime. This behaviour is codified as the energy gap law; in the vernacular of Marcus theory, it corresponds to the inverted region where $\lambda < |\Delta G_0|$. **b**, A large difference in the equilibrium geometries of the ground and excited states can lead to the opposite condition; that is, when $\lambda > |\Delta G_0|$, the excited-state lifetime decreases with increasing driving force as the FC overlap increases with an increase in zero-point energy difference. Often referred to as the inverse energy gap law, this phenomenology is identical to the Marcus normal region.

vibrational wavefunction of the excited state and excited vibrational wavefunctions of the ground state. As discussed in greater detail below, this phenomenology is identical to the so-called inverted region from the Marcus theory, wherein the rate constant decreases with increasing 'driving force' for the reaction (that is, ground-state recovery). In the case of compounds like $[Ru(bpy)_3]^{2+}$, where the equilibrium geometries of the ^{3}MLCT state and $^1A_1$ ground state are nearly identical[46], one does indeed observe an increase in excited-state lifetime with increasing excited-state energy, consistent with this picture[47–49].

The situation for Co(III) is fundamentally different due to the fact that the excited states driving the dynamics reflected in Fig. 1c are ligand-field in nature as opposed to charge-transfer. More specifically, because the ground state of a (nominally) octahedral, low-spin d^6 complex is characterized by a filled t_{2g} subshell, that is, $(t_{2g})^6$, all of the excited states associated with a low-spin, d^6 ground-state configuration will have electrons in the sigma anti-bonding e_g* orbitals. This will inexorably give rise to notable differences in the equilibrium geometries of the ground and excited states and is generally expected to lead to a picture more in line with that depicted in Fig. 2b. In this so-called inverse energy gap law regime (that is, the Marcus normal region), an increase in excited-state energy will lead to a faster rate of excited-state decay.

Variable-temperature time-resolved spectroscopy

While the data shown in Fig. 1c are strongly suggestive of Marcus-inverted-region behaviour, this result is not conclusive. One can envision circumstances across a series of compounds which, if the relative magnitudes of driving force (ΔG_0) and reorganization energy (λ) vary in just the correct manner, a trend like that shown in Supplementary Table 1 could arise (at least in principle). We sought to apply variable-temperature time-resolved spectroscopy to our series of Co(III) polypyridyl complexes both to substantiate our hypothesis concerning Marcus-inverted-region behaviour for the non-radiative ground-state recovery dynamics of this system and to identify its origin.

We have carried out these studies on four of the six members of the series, but for the sake of clarity we will provide a detailed discussion of the analysis of the data acquired for one member of the series—$[Co(pyrro\text{-}bpy)_3](PF_6)_3$—with the understanding that the same protocol was applied to the other compounds. The electronic absorption spectrum of $[Co(pyrro\text{-}bpy)_3](PF_6)_3$ collected in acetonitrile solvent is shown in Fig. 3a, superimposed on which is the spectral profile of the pump centred at 480 nm that was used for photoexcitation. As discussed above, the data acquired at 720 nm could be fit to a single-exponential kinetic model, yielding a time constant of 470 ± 20 ps, which was attributed to the relaxation of the lowest-energy excited state back to the ground state (Fig. 3c). The ground-state absorption feature centred near 350 nm is assigned to a $^1A_1 \rightarrow {}^1$LMCT absorption, which tails into the visible region and does overlap to some extent with the $^1A_1 \rightarrow {}^1T_1$ absorption that is our primary interest (Supplementary Fig. 2). To ensure that the ground-state recovery dynamics are indeed reflecting processes associated with the ligand-field manifold, we performed time-resolved absorption measurements as a function of excitation wavelength across the $^1A_1 \rightarrow {}^1T_1$ absorption envelope (Supplementary Fig. 3). On the high-energy side, this results in considerable absorption into the LMCT transition, while on the low-energy side the $^1T_1$ state is exclusively populated. While differences in the observed kinetics were noted at very early time delays (that is, <1 ps; Supplementary Fig. 4), the ground-state recovery dynamics were found to be independent of both excitation and probe wavelength (Supplementary Tables 2 and 3). This observation supports the notion that the process we are monitoring is indeed occurring between ligand-field excited state(s) and the ground state and does not involve the charge-transfer manifold in any way. Ground-state recovery dynamics of $[Co(pyrro\text{-}bpy)_3](PF_6)_3$ were acquired in a CH_3CN solution as a function of temperature in increments of 5 K between 258 K and 298 K following ligand-field photoexcitation (Fig. 3c); at each temperature point, the data were well described by simple, single-exponential kinetics.

Variable-temperature kinetics data can be modelled in a variety of ways depending on what sort of information is being sought. A detailed description of all the models used to fit variable-temperature data is in the Methods; in short, we used an Arrhenius model, simple transition state theory (that is, the Eyring equation) and semi-classical Marcus theory to understand the excited-state dynamics of this system.

The simplest of these is the Arrhenius model (equation (1)):

$$k_{nr} = A\exp\left(-\frac{E_a}{k_B T}\right) \quad (1)$$

https://doi.org/10.1038/s41557-024-01564-3

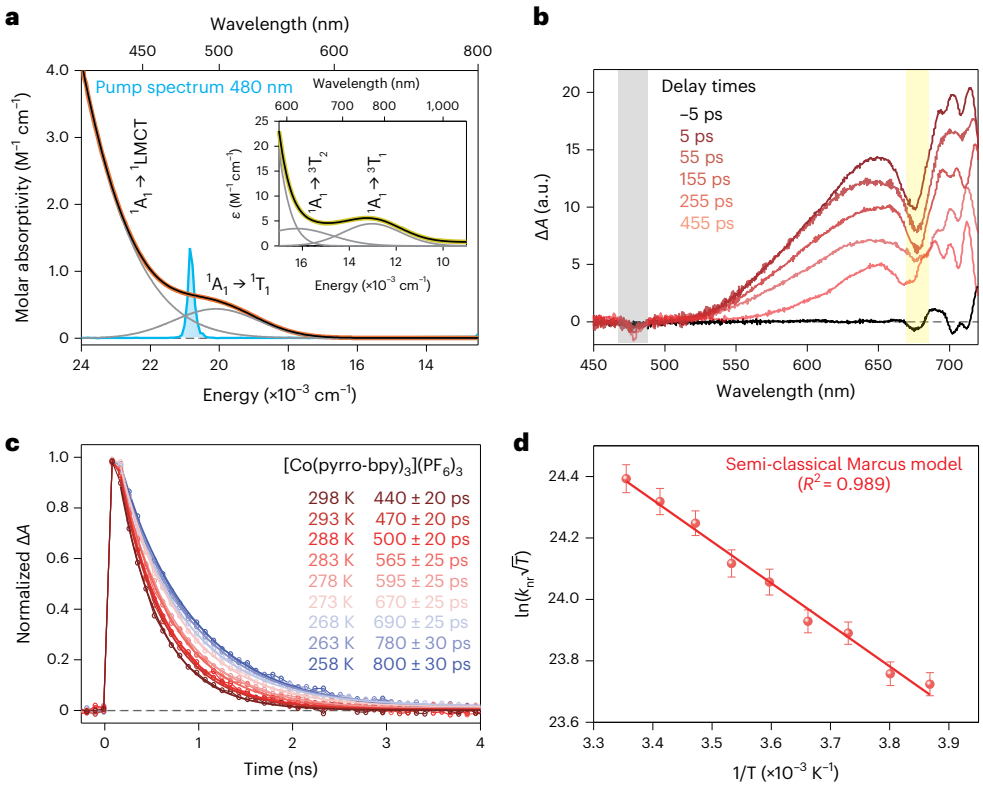

Fig. 3 | Variable-temperature transient absorption studies. Transient absorption and variable-temperature transient absorption data for [Co(pyrro-bpy)$_3$](PF$_6$)$_3$. **a**, Ground-state electronic absorption spectrum of [Co(pyrro-bpy)$_3$](PF$_6$)$_3$ in acetonitrile solution assigned to the spin-allowed (orange) $^1A_1 \rightarrow {}^1T_1$ ligand-field absorption band. The sharp feature superimposed on the spectrum represents the 480 nm excitation pulse, plotted in a manner reflecting the bandwidth of the pulse. The inset shows the spin-forbidden (yellow) $^1A_1 \rightarrow {}^3T_1$ and $^1A_1 \rightarrow {}^3T_2$ absorption bands of the same complex collected in acetonitrile using a cell with a 10 cm path length at higher solute concentration. The grey lines in both plots correspond to a Gaussian deconvolution of the spectrum, with the cumulative fit plotted in black. ε, molar absorptivity. CT, charge-transfer. **b**, Time-resolved absorption spectra for the complex acquired after 480 nm excitation in acetonitrile solution at room temperature. Delay times are shown in the inset. The signal in the grey shaded area is compromised by pump scatter at 480 nm, whereas that in the yellow shaded area is affected by a grating anomaly as indicated by its presence at the negative (that is, pre-pump) delay time. **c**, Transient absorption kinetics of the complex as a function of temperature, acquired at 720 nm subsequent to 480 nm photoexcitation in acetonitrile solution. **d**, Semi-classical Marcus type plot of the variable-temperature time-resolved absorption kinetic data for [Co(pyrro-bpy)$_3$](PF$_6$)$_3$ from **c**. The solid line corresponds to a fit of the data to semi-classical Marcus theory as formulated in equation (4). The errors bars represent s.d. that includes systematic error from three independent measurements. The text contains further details. R^2 is the coefficient of determination for the linear fit.

where k_{nr} is the non-radiative decay constant (that is, the observed decay constant k_{obs} for our non-emissive compounds), A is the pre-exponential factor (also known as the frequency factor), E_a is the activation energy and k_B and T are the Boltzmann constant and absolute temperature, respectively. As evident from the data in Fig. 3c, the time constant for ground-state recovery increases with decreasing temperature, indicating the presence of an activation energy for this process. Fitting the data for [Co(pyrro-bpy)$_3$]$^{3+}$ using equation (1), the activation energy was determined to be 850 ± 50 cm^{-1} (Supplementary Fig. 9). Considering that the so-called 'typical' reaction, in which a rate constant doubles upon increasing the temperature from 300 K to 310 K, corresponds to an Arrhenius activation energy of ~4,000 cm^{-1}, the value obtained for [Co(pyrro-bpy)$_3$]$^{3+}$ represents a small but nevertheless easily measurable barrier for ground-state recovery from the compound's lowest-energy ligand-field excited state.

The Eyring equation frames the relaxation process in terms of free energy of activation ($\Delta G^{\ddagger}$), thereby providing insight into the activation enthalpy ($\Delta H^{\ddagger}$) and entropy ($\Delta S^{\ddagger}$) associated with ground-state recovery according to equation (2):

$$k_{nr} = \kappa \frac{k_B T}{h} \exp\left(-\frac{\Delta G^{\ddagger}}{k_B T}\right) = \kappa \frac{k_B T}{h} \exp\left(\frac{\Delta S^{\ddagger}}{k_B}\right) \exp\left(-\frac{\Delta H^{\ddagger}}{k_B T}\right) \quad (2)$$

where κ is the transmission coefficient and h is Planck's constant. For [Co(pyrro-bpy)$_3$]$^{3+}$, the activation enthalpy and activation entropy were determined to be 655 ± 40 cm^{-1} and −3.30 ± 0.15 cm^{-1} K^{-1}, respectively (Supplementary Fig. 8).

More relevant to our discussion is the transformation of equation (2) into semi-classical Marcus theory, equation (3):

$$k_{nr} = \frac{2\pi}{\hbar} |H_{ab}|^2 \frac{1}{\sqrt{4\pi\lambda k_B T}} \exp\left[-\frac{(\Delta G_0 + \lambda)^2}{4\lambda k_B T}\right] \quad (3)$$

where ΔG_0 is driving force, λ represents reorganization energy, $\hbar$ is the reduced Planck's constant and H_{ab} is a constant that quantifies the electronic coupling between the two states involved in the process. Multiplying equation (3) through by $T^{1/2}$ and taking the natural log allows us to rearrange the semi-classical Marcus expression into a form more amenable for fitting variable-temperature data of the kind illustrated in Fig. 3c (equation (4)):

$$\ln\left(k_{nr}\sqrt{T}\right) = \ln\left(\frac{2\pi}{\hbar} |H_{ab}|^2 \frac{1}{\sqrt{4\pi\lambda k_B}}\right) - \left[\frac{(\Delta G_0 + \lambda)^2}{4\lambda k_B T}\right]. \quad (4)$$

https://doi.org/10.1038/s41557-024-01564-3

Table 1 | Arrhenius, Eyring and Marcus parameters associated with ground-state recovery from the lowest-energy ligand-field excited state of a series of Co(III) polypyridyl complexes

Complex	Ligand-field transition, $^1A_1 \rightarrow {}^3T_1$ (cm^{-1})	Arrhenius model	Eyring model	ΔG_0 (cm^{-1})[a]	Semi-classical Marcus model[b]	
		E_a (cm^{-1})	$\Delta S^{\ddagger}$ ($cm^{-1}K^{-1}$), $\Delta H^{\ddagger}$ (cm^{-1})		H_{ab} (cm^{-1})	λ (cm^{-1})
$[Co(pyrro\text{-}bpy)_3]^{3+}$	13,010	850±50	−3.30±0.15, 655±40	−10,100	25.5±1.0	5,700±500
$[Co(4,4'\text{-}OMebpy)_3]^{3+}$	13,650	1,050±50	−3.50±0.10, 900±30	−10,500	20.0±2.0	5,600±500
$[Co(4,4'\text{-}Br_2bpy)_3]^{3+}$	14,430	1,150±50	−3.80±0.15, 950±40	−10,650	18.2±1.5	5,500±500
$[Co(4,4'\text{-}deeb)_3]^{3+}$	14,910	1,200±50	−3.93±0.15, 1,010±40	−10,900	16.5±1.5	5,500±500

[a]ΔG_0 was obtained from DFT-derived single-point energy calculations on optimized ground and excited states. [b]H_{ab} and λ were obtained from fits of the experimental data to semi-classical Marcus theory (equation (4)) using the corresponding DFT-calculated ΔG_0 values.

Although the variable-temperature excited-state relaxation data for $[Co(pyrro\text{-}bpy)_3]^{3+}$ are clearly well described by equation (4), extracting specific values for these parameters is not possible from the fit alone as we have only two experimental observables (that is, k_{nr} and temperature) and three unknowns (ΔG_0, λ and H_{ab}). The ground-state absorption spectrum of the compound provides us with sufficient information to determine the energies of all of the ligand-field excited states, but these correspond to so-called vertical energies, not the zero-point energy of the structurally relaxed state that is relevant for assessing ΔG_0. Moreover, since these Co(III) complexes are non-emissive and the energies of ligand-field excited states cannot be approximated using electrochemistry in the same manner as charge-transfer states, there is no experimental probe at our disposal to determine the values of any of these parameters via an independent measurement. We must therefore look to theory to gain the insight necessary to analyse the data in Fig. 3d in greater depth.

Computational studies: assessing the Marcus parameters

Details concerning the density functional theory (DFT) calculations are provided in the Methods and Supplementary Section 10. Briefly, our approach involves computationally determining the zero-point free energy difference between the ground state and the lowest-energy ligand-field excited state (that is, ΔG_0): by combining this information with calculated vertical transition energies (benchmarked against our experimental ground-state absorption data; Methods), we can estimate the reorganization energy associated with ground-state recovery.

Regarding the identity of the lowest-energy ligand-field excited state, the two candidates based on inspection of the Tanabe–Sugano diagram we constructed for $[Co(pyrro\text{-}bpy)_3]^{3+}$ from the experimental electronic absorption spectrum (Extended Data Fig. 1) are the $^3T_1$ and $^5T_2$ ligand-field states. In this regard, it is important to note that not only is the activation entropy obtained from the Eyring analysis a negative number (Supplementary Fig. 8 and Table 1)—consistent with the expected decrease in molecular volume upon relaxation back to the low-spin ground state—the magnitude of $\Delta S^{\ddagger}$ of -3.30 ± 0.15 cm^{-1} is roughly half of what has been reported for isoelectronic Fe(II)-based spin-crossover complexes[50,51]. The fact that the latter corresponds to a conversion from a nominally $(t_2)^4(e^*)^2$ configuration to the $(t_2)^6(e^*)^0$ ground state, and that the $^3T_1$ state is best described as $(t_2)^5(e^*)^1$, suggests that the dynamics in our system involve the $^3T_1$ ligand-field excited state. Recently, the ligand-field state dynamics of the Co(III)-based tetra-metallic oxo cluster $[Co^{III}{}_4O_4](OAc)_4(py)_4$ (where OAc is acetate and py is pyridine) have been examined by Vura-Weis and coworkers using spin-sensitive $M_{2,3}$-edge X-ray absorption near-edge structure (XANES) spectroscopy[52]. The analysis of the ~80 ps ground-state recovery dynamics of that compound was most consistent with the lowest-energy excited state corresponding to the $^3T_1$ state. The magnitude of the ligand-field splitting parameter 10Dq for this compound was determined to be 17,100 cm^{-1}, which is smaller than the 10Dq values for all of the Co(III) polypyridyl complexes we have examined.

As will become evident in the sections to follow, we do believe that the lowest-energy excited state of $[Co(pyrro\text{-}bpy)_3]^{3+}$ (as well as the other members of the series) is indeed the $^3T_1$ state, a conclusion that has important implications for explaining the behaviour we observe concerning the ground-state recovery dynamics of these compounds. For the sake of clarity, we will therefore proceed with the analysis to follow based on such an assignment; however, a parallel analysis assuming the $^5T_2$ state (which leads to internally inconsistent conclusions) is provided in Supplementary Section 12.

The driving force is straightforward to calculate, since it is simply the difference in energy between the equilibrium structures of the ground and excited ligand-field states in question: for $[Co(pyrro\text{-}bpy)_3]^{3+}$, a value of $-10{,}100 \pm 550$ cm^{-1} is found for the $^3T_1$ state, indicating that the zero-point energy of the structurally relaxed $^3T_1$ state sits 10,100 cm^{-1} above the ground state (Methods for details). Using this value for ΔG_0, we can now deconvolve the two contributions to the slope of the $\ln(k_{nr}\sqrt{T})$ versus $1/T$ plot shown in Fig. 3d. The quadratic nature of the exponential term gives two possible values for the reorganization energy: $\lambda = 18{,}400 \pm 600$ cm^{-1} and $\lambda = 5{,}700 \pm 500$ cm^{-1}. Clearly, the second solution is very much in line with the one derived from the calculations (Methods), particularly when one considers the fact that the calculated value of 3,000 cm^{-1} corresponds only to the inner-sphere portion of the total reorganization energy (that is, structural changes of the molecule only), whereas the experimental value of λ will reflect both inner-sphere and outer-sphere (that is, solvent) contributions. Additional guidance can be gleaned from other experimental reports concerning reorganization energies on different (but related) chemical systems (Supplementary Section 11)[53]. Our experimental data, when combined with the results from our DFT calculations, therefore lead to the conclusion that $\lambda = 5{,}700 \pm 500$ cm^{-1} is the correct solution for the fit shown in Fig. 3d. When this value is combined with the driving force of $-10{,}100 \pm 550$ cm^{-1}, we can state with a high degree of confidence that the relaxation dynamics of $[Co(pyrro\text{-}bpy)_3]^{3+}$ lie firmly in the Marcus inverted region, where $\lambda < |\Delta G_0|$.

The preceding discussion focused almost exclusively on the properties of $[Co(pyrro\text{-}bpy)_3]^{3+}$, but analogous studies were carried out on three additional members of the series of compounds shown in Fig. 1a: these data are summarized in Table 1. Inspection of the data shows remarkable consistency in the magnitude of the reorganization energy. Given the fact that compositional changes in the molecule involve substitutions on the periphery of the bipyridyl rings (that is, relatively removed from the primary coordination sphere about the metal centre), this invariance in the fitted value of λ bolsters our confidence in the veracity of our analysis. Variations in the lifetime at room temperature were alluded to previously in this Article, but now in addition we see that the Arrhenius activation energy shows a systematic increase with increasing zero-point energy difference between the ground state and lowest-lying excited state. This is precisely the phenomenology one would expect in the Marcus inverted region, that is, an increasing barrier (and thus a longer excited-state lifetime) as the driving force for the increases in reaction.

https://doi.org/10.1038/s41557-024-01564-3

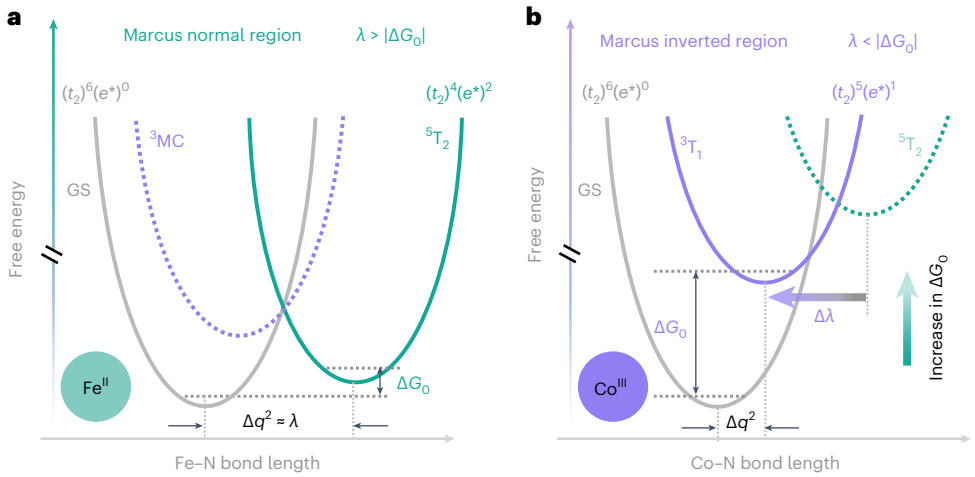

Fig. 4 | Origin of Marcus inverted region in Co(III). a,**b**, Schematic representation of the relative change in the excited-state geometry and driving force for the ground-state recovery process from Fe(II) (**a**) to Co(III) (**b**) polypyridyl complexes. The combination of increased driving force and reduced reorganization energy for the latter is what gives rise to Marcus-inverted-region behaviour for the Co(III) complexes examined in this study.

Origin of the inverted-region behaviour

Since the intercept from equation (4) is proportional to $|H_{ab}|^2/\sqrt{\lambda}$, a reliable value for λ now allows us to estimate the magnitude of electronic coupling between the $^3T_1$ and $^1A_1$ states as 25.5 ± 1.0 cm^{-1}; the (relatively) high degree of precision for this number stems from the quartic relationship between H_{ab} and λ, giving rise to a fairly narrow range of values for H_{ab} that are consistent with the experimental data. We note that this is substantially larger than what has been reported for excited-state/ground-state coupling in Fe(II) polypyridyls (~5 cm^{-1}; ref. 54), a fact that we believe adds critical support to our assignment of the $^3T_1$ term as the lowest-energy excited state of $[Co(pyrro\text{-}bpy)_3]^{3+}$.

It is not only the increase in the magnitude of H_{ab} relative to what is observed for Fe(II) analogues that we consider important, but also the trend we observe as a function of driving force. As indicated previously, it is well-established that the ground-state recovery process in Fe(II) polypyridyl complexes corresponds to a $^5T_2 \rightarrow {}^1A_1$ conversion, a process wherein the spin of the system changes by two units (that is, $S = 2$ for the $^5T_2$ excited state to $S = 0$ for the $^1A_1$ ground state). There is no matrix element that allows one to directly couple two electronic states that differ by two spin quanta, so the coupling needed to effect ground-state recovery in these systems represents a second-order interaction whereby the $^5T_2$ state couples with a (non-thermally accessed) $S = 1$ state (for example, the $^3T_1$ state), which in turn couples to the $S = 0$ ground state. Because of the combined effect of the second-order coupling and the relative energy differences between the $^5T_2/{}^3T_1$ and $^3T_1/{}^1A_1$ gaps (Extended Data Fig. 1), the magnitude of H_{ab} is (1) small and (2) expected to slightly increase with increasing ligand-field strength. This is clearly at odds with the data obtained on our series of Co(III) complexes listed in Table 1, which necessitates that another mechanism must be considered.

Carrying out the same analysis for relaxation proceeding from the $^3T_1$ state, the expected trend in H_{ab} is fundamentally different. First, one can directly couple states characterized by $S = 1$ and $S = 0$, so the magnitude of the interaction will be intrinsically larger than a second-order interaction (at least qualitatively). More importantly, the fact that the two states would be directly interacting with each other means that the trend in the magnitude of the coupling constant should conform to simple perturbation theory; that is, as the states get further apart in energy, the degree to which they interact should decrease. This is precisely what we observe when we look at the value of H_{ab} as a function of 10Dq: as the ligand-field strength increases across the series, the magnitude of H_{ab} systematically decreases. This trend indicates the presence of direct coupling between the ground state and the lowest-energy excited state in these Co(III) polypyridyl compounds. We view this as additional compelling evidence that the ground-state recovery dynamics of these chromophores do, indeed proceed from the $^3T_1$ ligand-field excited state.

With this assignment in hand, we can now consider its consequence with regard to Marcus-normal-region versus Marcus-inverted-region behaviour. We have previously demonstrated that, all other things being equal, replacement of Fe(II) for Co(III) results in an ~3,000 cm^{-1} increase in the magnitude of 10Dq (ref. 29). This corresponds to a shift to the right in the context of a Tanabe–Sugano diagram but more importantly as a vertical displacement of the zero-point energy of the lowest-energy excited state when viewed in terms of potential energy surfaces (Fig. 4). If the excited electronic state of a given Co(III) complex was the same as for its Fe(II) analogue, the reorganization energy associated with excited-state relaxation would be expected to be roughly the same. Put another way, if the horizontal displacement of the ground-state and excited-state potential energy surfaces—which is a proxy for the reorganization energy—was unperturbed, whether the increase in 10Dq would be sufficient to transition from the Marcus-normal-region behaviour to the inverted behaviour that we observe (Fig. 4a) would be an open question. However, the increase in 10Dq is only part of the story. As mentioned previously, the $^5T_2$ state derives from a $(t_2)^4(e^*)^2$ configuration, whereas the $^3T_1$ state corresponds to $(t_2)^5(e^*)^1$ configuration. The reduction in sigma anti-bonding character of the latter is the reason why the reorganization energy determined for the Co(III) complexes is roughly half of that found for Fe(II). What this means in the context of the potential energy surface diagram for the system is a diagonal shift in the relative position of the lowest-energy excited state, that is, an increase in zero-point energy coupled with a decrease in the horizontal separation between the two potentials (Fig. 4b). Our assessment of the situation for ground-state recovery in the Co(III) complexes studied herein is summarized in Fig. 5.

Conclusions

Variable-temperature ultrafast time-resolved absorption spectroscopy has been combined with DFT in an effort to understand the origin of the photophysical behaviour associated with ground-state recovery dynamics of a series of Co(III) tris-bipyridyl complexes. The experimental data were analysed through the lens of non-radiative decay theories ranging from a simple Arrhenius model to semi-classical Marcus theory.

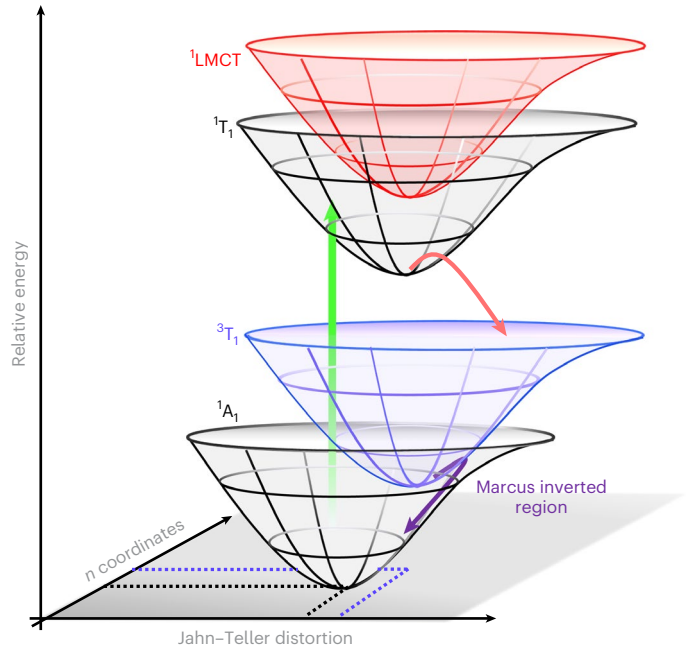

Fig. 5 | Proposed model. Schematic representation of the potential energy surface diagram for the excited-state relaxation process of Co(III) tris-bipyridyl complexes subsequent to $^1A_1 \rightarrow {}^1T_1$ ligand-field photoexcitation. Ground-state recovery dynamics proceed from the $^3T_1$ ligand-field excited state with a balance of free energy difference and reorganization energy that places the process firmly in the Marcus inverted region. The n-coordinates represent all potential normal mode vibrations which are not coupled to Jahn–Teller distortion coordinate and the dotted lines are used to show the structural changes and the solid arrows represent the state conversion process after photoexcitation.

When combined with the results of DFT calculations benchmarked with experimental spectroscopic data, values for the driving force (ΔG_0) and reorganization energy (λ) were obtained that indicated the magnitude of ΔG_0 across the series was nearly twofold larger than the reorganization energy, thereby confirming Marcus-inverted-region behaviour. Moreover, both the magnitude of H_{ab} and its variation as a function of driving force strongly implicated the $^3T_1$ ligand-field excited state as the lowest-energy excited state of all compounds in the series, in contrast to the $^5T_2$ state in isoelectronic Fe(II) polypyridyls. This change in the nature of the lowest-energy excited state—which leads to smaller reorganization energies—coupled with a larger zero-point energy difference conspire to place the excited-state relaxation dynamics of Co(III) polypyridyl complexes in the Marcus inverted region.

While there is clearly room for improvement in certain aspects of this class of chromophores when considering future applications (for example, increased absorption cross-sections, excitation wavelengths that extend to longer wavelengths in the visible and enhanced excited-state lifetimes, to name a few)[55], we believe that the fundamental photophysical properties of these simple Co(III) polypyridyl complexes that we have delineated in this report can serve as a roadmap for designing next generation photocatalysts that can leverage new opportunities afforded by accessing the Marcus inverted region in this manner.

Online content

Any methods, additional references, Nature Portfolio reporting summaries, source data, extended data, supplementary information, acknowledgements, peer review information; details of author contributions and competing interests; and statements of data and code availability are available at https://doi.org/10.1038/s41557-024-01564-3.

References

1. Juris, A. et al. Ru(II) polypyridine complexes: photophysics, photochemistry, eletrochemistry, and chemiluminescence. *Coord. Chem. Rev.* **84**, 85–277 (1988).
2. Dixon, I. M. et al. A family of luminescent coordination compounds: iridium(III) polyimine complexes. *Chem. Soc. Rev.* **29**, 385–391 (2000).
3. Lytle, F. E. & Hercules, D. M. Luminescence of tris (2,2′-bipyridine) ruthenium(II) dichloride. *J. Am. Chem. Soc.* **646**, 253–257 (1968).
4. Arias-Rotondo, D. M. & McCusker, J. K. The photophysics of photoredox catalysis: a roadmap for catalyst design. *Chem. Soc. Rev.* **45**, 5803–5820 (2016).
5. de Groot, L. H. M., Ilic, A., Schwarz, J. & Wärnmark, K. Iron photoredox catalysis–past, present, and future. *J. Am. Chem. Soc.* **145**, 9369–9388 (2023).
6. Twilton, J. et al. The merger of transition metal and photocatalysis. *Nat. Rev. Chem.* **1**, 0052 (2017).
7. McCusker, J. K. Electronic structure in the transition metal block and its implications for light harvesting. *Science* **363**, 484–488 (2019).
8. Wegeberg, C. & Wenger, O. S. Luminescent first-row transition metal complexes. *JACS Au* **1**, 1860–1876 (2021).
9. Beaudelot, J. et al. Photoactive copper complexes: properties and applications. *Chem. Rev.* **122**, 16365–16609 (2022).
10. Sinha, N., Wegeberg, C., Häussinger, D., Prescimone, A. & Wenger, O. S. Photoredox-active Cr(0) luminophores featuring photophysical properties competitive with Ru(II) and Os(II) complexes. *Nat. Chem.* **15**, 1730–1736 (2023).
11. Herr, P., Kerzig, C., Larsen, C. B., Häussinger, D. & Wenger, O. S. Manganese(I) complexes with metal-to-ligand charge transfer luminescence and photoreactivity. *Nat. Chem.* **13**, 956–962 (2021).
12. Smeigh, A. L., Creelman, M., Mathies, R. A. & McCusker, J. K. Femtosecond time-resolved optical and Raman spectroscopy of photoinduced spin crossover: temporal resolution of low-to-high spin optical switching. *J. Am. Chem. Soc.* **130**, 14105–14107 (2008).
13. McCusker, J. K. et al. Subpicosecond ^{1}MLCT→$^5T_2$ intersystem crossing of low-spin polypyridyl ferrous complexes. *J. Am. Chem. Soc.* **115**, 298–307 (1993).
14. McCusker, J. K., Rheingold, A. L. & Hendrickson, D. N. Variable-temperature studies of laser-initiated $^5T_2 \rightarrow {}^1A_1$ intersystem crossing in spin-crossover complexes: empirical correlations between activation parameters and ligand structure in a series of polypyridyl ferrous complexes. *Inorg. Chem.* **35**, 2100–2112 (1996).
15. Monat, J. E. & McCusker, J. K. Femtosecond excited-state dynamics of an iron(II) polypyridyl solar cell sensitizer model. *J. Am. Chem. Soc.* **122**, 4092–4097 (2000).
16. Bressler, C. et al. Femtosecond XANES study of the light-induced spin crossover dynamics in an iron(II) complex. *Science* **323**, 489–492 (2009).
17. Zhang, K., Ash, R., Girolami, G. S. & Vura-Weis, J. Tracking the metal-centered triplet in photoinduced spin crossover of $[Fe(phen)_3]^{2+}$ with tabletop femtosecond M-edge X-ray absorption near-edge structure spectroscopy. *J. Am. Chem. Soc.* **141**, 17180–17188 (2019).
18. Kitzmann, W. R. & Heinze, K. Charge-transfer and spin-flip states: Thriving as complements. *Angew. Chem. Int. Ed.* **62**, 1–17 (2023).
19. Dorn, M. et al. in *Comprehensive Inorganic Chemistry III* 3rd edn, 707–788 (Elsevier, 2023).
20. Zhang, W. et al. Tracking excited-state charge and spin dynamics in iron coordination complexes. *Nature* **509**, 345–348 (2014).

21. Woodhouse, M. D. & McCusker, J. K. Mechanistic origin of photoredox catalysis involving iron(II) polypyridyl chromophores. *J. Am. Chem. Soc.* **142**, 16229–16233 (2020).
22. Liu, Y. et al. Towards longer-lived metal-to-ligand charge transfer states of iron(II) complexes: an *N*-heterocyclic carbene approach. *Chem. Commun.* **49**, 6412–6414 (2013).
23. Fredin, L. A. et al. Exceptional excited-state lifetime of an iron(II)–*N*-heterocyclic carbene complex explained. *J. Phys. Chem. Lett.* **5**, 2066–2071 (2014).
24. Chábera, P. et al. Fe^{II} hexa *N*-heterocyclic carbene complex with a 528 ps metal-to-ligand charge-transfer excited-state lifetime. *J. Phys. Chem. Lett.* **9**, 459–463 (2018).
25. Paulus, B. C., Nielsen, K. C., Tichnell, C. R., Carey, M. C. & McCusker, J. K. A modular approach to light capture and synthetic tuning of the excited-state properties of Fe(II)-based chromophores. *J. Am. Chem. Soc.* **143**, 8086–8098 (2021).
26. Mukherjee, S., Bowman, D. N. & Jakubikova, E. Cyclometalated Fe(II) complexes as sensitizers in dye-sensitized solar cells. *Inorg. Chem.* **54**, 560–569 (2015).
27. Braun, J. D. et al. Iron(II) coordination complexes with panchromatic absorption and nanosecond charge-transfer excited state lifetimes. *Nat. Chem.* **11**, 1144–1150 (2019).
28. Steube, J. et al. Excited-state kinetics of an air-stable cyclometalated iron(II) complex. *Chem. Eur. J.* **25**, 11826–11830 (2019).
29. Yarranton, J. T. & McCusker, J. K. Ligand-field spectroscopy of Co(III) complexes and the development of a spectrochemical series for low-spin d^6 charge-transfer chromophores. *J. Am. Chem. Soc.* **144**, 12488–12500 (2022).
30. Alowakennu, M. M., Ghosh, A. & McCusker, J. K. Direct evidence for excited ligand field state-based oxidative photoredox chemistry of a cobalt(III) polypyridyl photosensitizer. *J. Am. Chem. Soc.* **145**, 20786–20791 (2023).
31. Kalsi, D., Dutta, S., Barsu, N., Rueping, M. & Sundararaju, B. Room-temperature C–H bond functionalization by merging cobalt and photoredox catalysis. *ACS Catal.* **8**, 8115–8120 (2018).
32. Pal, A. K., Li, C., Hanan, G. S. & Zysman-Colman, E. Blue-emissive cobalt(III) complexes and their use in the photocatalytic trifluoromethylation of polycyclic aromatic hydrocarbons. *Angew. Chem. Int. Ed.* **57**, 8027–8031 (2018).
33. Zhang, P. et al. Mass production of a single-atom cobalt photocatalyst for high-performance visible-light photocatalytic CO_2 reduction. *J. Mater. Chem. A* **9**, 26286–26297 (2021).
34. Zhang, G. et al. External oxidant-free oxidative cross-coupling: a photoredox cobalt-catalyzed aromatic C–H thiolation for constructing C–S bonds. *J. Am. Chem. Soc.* **137**, 9273–9280 (2015).
35. Chan, A. Y. et al. Exploiting the Marcus inverted region for first-row transition metal-based photoredox catalysis. *Science* **382**, 191–197 (2023).
36. Langford, C. H., Group, H. E., Malkhasian, A. Y. S. & Sharma, D. K. Subnanosecond transients in the spectra of cobalt(III) amine complexes. *J. Am. Chem. Soc.* **106**, 2727–2728 (1984).
37. Ferrari, L. et al. A fast transient absorption study of Co(AcAc)3. *Front. Chem.* 7, https://doi.org/10.3389/fchem.2019.00348 (2019).
38. Kaufhold, S. et al. Microsecond photoluminescence and photoreactivity of a metal-centered excited state in a hexacarbene–Co(III) complex. *J. Am. Chem. Soc.* **143**, 1307–1312 (2021).
39. Gray, B. & Beach, N. A. The electronic structures of octahedral metal complexes. I. Metal hexacarbonyls and hexacyanides. *J. Am. Chem. Soc.* **85**, 2922–2927 (1963).
40. Miskowski, V. M., Gray, H. B., Wilson, R. B. & Solomon, E. I. Position of the $^3T_{1g} \leftarrow {}^1A_{1g}$ transition in hexacyanocobaltate(III). Analysis of absorption and emission results. *Inorg. Chem.* **18**, 1410–1412 (1978).
41. McCusker, J. K., Walda, K. N., Magde, D. & Hendrickson, D. N. Picosecond excited-state dynamics in octahedral cobalt(III) complexes: intersystem crossing versus internal conversion. *Inorg. Chem.* **32**, 394–399 (1993).
42. Viaene, L., D'Olieslager, J., Ceulemans, A. & Vanquickenborne, L. G. Excited-state spectroscopy of hexacyanocobaltate(III). *J. Am. Chem. Soc.* **101**, 1405–1409 (1979).
43. Sinha, N., Wegeberg, C., Prescimone, A. & Wenger, O. S. Cobalt(III) carbene complex with an electronic excited-state structure similar to cyclometalated iridium(III) compounds. *J. Am. Chem. Soc.* **144**, 9859–9873 (2022).
44. Caspar, J. V., Kober, E. M., Sullivan, B. P. & Meyer, T. J. Application of the energy gap law to the decay of charge-transfer excited states. *J. Am. Chem. Soc.* **104**, 91–95 (1982).
45. Englman, R. & Jortner, J. The energy gap law for radiationless transitions in large molecules. *Mol. Phys.* **18**, 285–287 (1970).
46. Bressler, C. & Chergui, M. Ultrafast X-ray absorption spectroscopy. *Chem. Rev.* **104**, 1781–1812 (2004).
47. Damrauer, N. H., Boussie, T. R., Devenney, M. & McCusker, J. K. Effects of intraligand electron delocalization, steric tuning, and excited-state vibronic coupling on the photophysics of aryl-substituted bipyridyl complexes of Ru(II). *J. Am. Chem. Soc.* **119**, 8253–8268 (1997).
48. Strouse, G. F. et al. Influence of electronic delocalization in metal-to-ligand charge transfer excited states. *Inorg. Chem.* **34**, 473–487 (1995).
49. Bozzi, A. S. & Rocha, W. R. Calculation of excited state internal conversion rate constant using the one-effective mode Marcus-Jortner-Levich theory. *J. Chem. Theory Comput.* **19**, 2316–2326 (2023).
50. Al-Obaidi, A. H. R. et al. Structural and kinetic studies of spin crossover in an iron(II) complex with a novel tripodal ligand. *Inorg. Chem.* **35**, 5055–5060 (1996).
51. McGarvey, J. J., Lawthers, I., Heremans, K. & Toftlund, H. Spin-state relaxation dynamics in iron(II) complexes: solvent on the activation and reaction and volumes for the $^1A \rightleftharpoons {}^5T$ interconversion. *J. Chem. Soc. Chem. Commun.* **29**, 1575–1576 (1990).
52. Shari'Ati, Y. & Vura-Weis, J. Ballistic $\Delta S = 2$ intersystem crossing in a cobalt cubane following ligand-field excitation probed by extreme ultraviolet spectroscopy. *Phys. Chem. Chem. Phys.* **23**, 26990–26996 (2021).
53. Xie, Y., Baillargeon, J. & Hamann, T. W. Kinetics of regeneration and recombination reactions in dye-sensitized solar cells employing cobalt redox shuttles. *J. Phys. Chem. C* **119**, 28155–28166 (2015).
54. Carey, M. C., Adelman, S. L. & McCusker, J. K. Insights into the excited state dynamics of Fe(II) polypyridyl complexes from variable-temperature ultrafast spectroscopy. *Chem. Sci.* **10**, 134–144 (2019).
55. Yaltseva, P. & Wenger, O. S. Photocatalysis gets energized by abundant metals. *Science* **382**, 153–154 (2023).

Methods

Variable-temperature transient absorption spectroscopy

Variable-temperature kinetic data can be modelled in a variety of ways depending on what sort of information is being sought. While the specific expressions stemming from these various models differ, those reliant on the Born–Oppenheimer approximation all have the general form shown in equation (5):

$$k_{nr} = C \times T^{n} \exp\left(-\frac{\Delta E}{k_B T}\right) \quad (5)$$

where the rate constant is expressed as the product of (1) an electronic term $C \times T^n$ (where C is a constant(s) and the value of n is model dependent) and (2) a nuclear term, which is associated with a barrier (ΔE) that follows Boltzmann-like statistics. The simplest of these is the Arrhenius model shown in equation (1), where k_{nr} is the non-radiative decay constant, A is the pre-exponential factor (also known as the frequency factor), E_a is the activation energy and k_B and T are the Boltzmann constant and absolute temperature, respectively; referencing back to equation (1), this model is obtained for $n = 0$. A plot of $\ln(k_{nr})$ versus $1/T$ yields a straight line with an intercept of $\ln(A)$ and slope corresponding to $-E_a/k_B$.

While the Arrhenius model provides useful information concerning the potential energy landscape associated with excited-state relaxation, its empirical nature prevents more detailed insight into the electronic structure of the compound that gives rise to those fitted parameters. The next level of sophistication is transition state theory, which can be derived from statistical mechanics and recasts the parameters describing temperature-dependent kinetics in terms of free energy. The Eyring equation, shown in equation (2), breaks the problem down in terms of enthalpies and entropies and corresponds to $n = 1$ in equation (1). A plot of $\ln(k_{nr}/T)$ versus $1/T$ again yields a linear relationship with a slope now defined by the activation enthalpy ($\Delta H^{\ddagger}$), while the intercept reflects a convolution of the activation entropy ($\Delta S^{\ddagger}$) and the so-called transmission coefficient (κ). The latter is often assumed to have a value of 1, which allows for a determination of $\Delta S^{\ddagger}$ and corresponds to the adiabatic limit in the vernacular of non-radiative decay theory.

More relevant to our discussion is the transformation of equation (2) into semi-classical Marcus theory, wherein the activation free energy is replaced by the well-known Marcus relation that considers the combined influence of driving force (ΔG_0) and reorganization energy (λ) in the nuclear term and introduces the Landau–Zener formalism[56] to treat the electronic term quantum mechanically. This expression is shown in equation (3) where H_{ab} is a constant that quantifies the electronic coupling between the two states involved in the process. Although Marcus theory was originally developed to describe outer-sphere electron-transfer processes, it is actually just a special case of the more general non-radiative decay theory and has been successfully applied to understand non-radiative kinetic processes in a wide variety of settings, including excited-state relaxation in transition metal complexes[57,58]. According to Marcus theory, the non-radiative rate constant has a quadratic relationship with driving force and reorganization that gives rise to three distinct regimes of behaviour. When the driving force is smaller in magnitude than the amount of energy required to structurally reorganize the system from the equilibrium configuration of the excited state to that of the ground state (that is, when $|\Delta G_0| < \lambda$; Fig. 2b), k_{nr} increases with increasing zero-point energy difference. This is referred to as the 'normal' region and corresponds to our intuition that, as the thermodynamic favourability of the reaction increases, the rate constant for the reaction also increases; this regime also corresponds to the 'inverse energy gap law' alluded to previously. When the free energy difference becomes equal in magnitude to the reorganization energy, the exponential term in equation (3) collapses to unity and the rate constant is dictated primarily by the electronic coupling between the two states (H_{ab}). This is the 'barrierless' region and is characterized by a very weak, inverted temperature dependence in the rate constant that scales as $T^{-1/2}$. Further increase in the driving force lead to the counterintuitive result of reintroducing the barrier: this is the 'inverted region' (that is, the energy gap law), where the rate constant starts to decrease again as the exergonicity of the reaction increases (that is, Fig. 2a). This is the revolutionary idea that Marcus presented more than 70 years ago[59] that was ultimately verified in the classic work of Closs and Miller[60,61]. We note that the overall form of equation (3) is again reminiscent of equation (5) for $n = -½$ and a barrier described by the now well-known Marcus relation of $(\Delta G_0 + \lambda)^2/4\lambda$.

Multiplying equation (3) through by $T^{1/2}$ and taking the natural log allows us to rearrange the semi-classical Marcus expression into a form more amenable for fitting variable-temperature data of the kind illustrated in Fig. 3c. This expression is shown in equation (4), where a plot of $\ln(k_{nr}\sqrt{T})$ versus $1/T$ produces the linear correlation shown in Fig. 3d. Equation (4) indicates that the slope of the plot contains information related to the driving force, ΔG_0, which equates to the zero-point energy difference between the lowest-energy ligand-field excited state and the ground state, and the reorganization energy λ, which informs on the difference in the equilibrium geometries between those two states. The reorganization energy also contributes to the value of the intercept, although this parameter from the fit is dominated by the magnitude of the electronic coupling (H_{ab}).

Computational details for assessing reorganization energy

The geometry of the singlet ground state of $[Co(pyrro\text{-}bpy)_3]^{3+}$ was optimized using the B3LYP functional and incorporating empirical dispersion corrections (that is, B3LYP + D2). The optimized structure compared favourably with the experimentally determined single-crystal X-ray structure[29], with average Co–N bond lengths that differed on the order of only 1% between the experimental and optimized structures. Equilibrium geometries for the lowest-energy triplet and quintet spin states, which will ultimately allow us to assess relative zero-point energies of the excited states, were also optimized. As expected, both are ligand-field in nature as illustrated in the spin density map shown in Extended Data Fig. 1b (inset) and Supplementary Fig. 17f. The optimized triplet geometry was found to be Jahn–Teller distorted, consistent with expectations for a multielectronic term state deriving from a $(t_2)^5(e^*)^1$ configuration. The equilibrium geometry of the quintet state was found to be more symmetric, again consistent with the $(t_2)^4(e^*)^2$ configuration, where the degeneracy needed to effect a Jahn–Teller distortion exists only in the weakly anti-bonding π-symmetry t_2 orbitals. Additional details concerning these optimized geometries can be found in Supplementary Table 7.

Since it is well known that the inclusion of Hartree–Fock (HF) exchange preferentially stabilizes high-spin configurations[62], we sought to create tailored B3LYP functionals by taking advantage of the experimental data we possessed on the electronic structure of $[Co(pyrro\text{-}bpy)_3]^{3+}$ from steady-state absorption spectroscopy. Using the experimentally determined $^1A_1 \rightarrow {}^1T_1$ and spin-forbidden $^1A_1 \rightarrow {}^3T_1$ absorption maxima as reference points, we carried out calculations in which the percentage of HF exchange incorporated into the functional was varied in the range of 0–30%. As shown in Extended Data Fig. 1c, we found that for $[Co(pyrro\text{-}bpy)_3]^{3+}$, inclusion of 20% HF exchange (which corresponds to the unmodified B3LYP functional) resulted in the best agreement between experiment and the calculated vertical energies; 20% also proved to be optimal for the other members of the series. Single-point energies on the geometry-optimized structures were therefore calculated using 20% HF exchange to obtain computed zero-point free energies for the $^1A_1$, $^3T_1$ and $^5T_2$ states. These calculations indicated that the $S = 1$ state was the lowest-energy excited state, with the $S = 2$ (that is, $^5T_2$) state lying substancially higher.

The reorganization energy was described by Marcus as the amount of energy required to modify the geometry of the system from that of

the initial state to that of the final state without actually undergoing the transformation. Conceptually, this equates to moving along the potential energy surface corresponding to the 'reactant' (in our case the lowest-energy ligand-field excited state) from its equilibrium geometry at the minimum of its potential energy surface to a configuration corresponding to the equilibrium geometry of the 'product' (that is, the ground state). This can be simulated computationally by simply taking the difference between the optimized, zero-point energy of the excited ligand-field state at its equilibrium geometry and the energy of that same electronic state upon excitation from the ground state (that is, the Franck–Condon state). The latter can be determined computationally but is also available for our compounds experimentally, as it corresponds to the 770 nm maximum of the $^1A_1 \rightarrow {}^3T_1$ absorption feature observed in the compound's electronic absorption spectrum (Fig. 3a, inset)[29]. Both of these approaches yield a very similar value of ~3,000 cm^{-1} (0.37 eV; Supplementary Table 9). We note that these calculated differences are virtually insensitive to the percentage of HF exchange incorporated into the functional (Extended Data Fig. 1c), an observation that provides us with added confidence in the conclusions being drawn from the calculations.

To gain further insight into the degree to which the solvent may be influencing the excited-state dynamics in our system, we carried out measurements on $[Co(pyrro\text{-}bpy)_3]^{3+}$ in a series of different solvents covering a broad range of static dielectric constants (for example, from 9.00 for dichloromethane to 47.24 for dimethyl sulfoxide). As expected, the ligand-field absorption band ($^1A_1 \rightarrow {}^1T_1$) was found to be largely insensitive to changes in the solvent due to its localization on the metal centre (Supplementary Fig. 6). The normalized transient absorption kinetic traces following photoexcitation at 510 nm are shown in Supplementary Fig. 6b; a plot of ground-state recovery time constants as a function of static dielectric constant as well as solvent polarizability are shown in Supplementary Fig. 6c,d, respectively. The data, while not exhibiting a strong correlation to either of these macroscopic solvent properties, reveal variations in the kinetics suggestive of a small but nevertheless measurable contribution to the total reorganization energy for ground-state recovery from the solvent. This is qualitatively consistent with our previously published study on the influence of outer-sphere reorganization on ground-state recovery dynamics of $[Fe(bpy)_3]^{2+}$, where a contribution from the solvent was attributed to differences in solvation due to the large volume change associated with the high-spin to low-spin conversion[63].

Data availability

All the data that support the findings of this study are provided via Figshare at https://doi.org/10.6084/m9.figshare.25803085 (ref. 64). Source data are provided with this paper.

References

56. Zener, C. Non-adiabatic crossing of energy levels. *Proc. R. Soc. Lond. A* **132**, 696–702 (1932).
57. Sutin, N. Nuclear, electronic, and frequency factors in electron-transfer reactions. *Acc. Chem. Res.* **15**, 275–282 (1982).
58. Buhks, E., Navon, G., Bixon, M. & Jortner, J. Spin conversion processes in solutions. *J. Am. Chem. Soc.* **102**, 2918–2923 (1980).
59. Marcus, R. A. On the theory of oxidation-reduction reactions involving electron transfer. I. *J. Chem. Phys.* **24**, 966–978 (1956).
60. Miller, J. R., Calcaterra, L. T. & Closs, G. L. Intramolecular long-distance electron transfer in radical anions. The effects of free energy and solvent on the reaction rates. *J. Am. Chem. Soc.* **106**, 3047–3049 (1984).
61. Closs, G. L. & Miller, J. R. Intramolecular long-distance electron transfer in organic molecules. *Science* **240**, 440–447 (1988).
62. Bowman, D. N. & Jakubikova, E. Low-spin versus high-spin ground state in pseudo-octahedral iron complexes. *Inorg. Chem.* **51**, 6011–6019 (2012).
63. Miller, J. N. & McCusker, J. K. Outer-sphere effects on ligand-field excited-state dynamics: solvent dependence of high-spin to low-spin conversion in $[Fe(bpy)_3]^{2+}$. *Chem. Sci.* **11**, 5191–5204 (2020).
64. Ghosh, A., Yarranton, J. T. & McCusker, J. K. Data for 'Establishing the origin of Marcus-inverted-region behavior in the excited-state dynamics of cobalt(III) polypyridyl complexes'. *Figshare* https://doi.org/10.6084/m9.figshare.25803085 (2024).

Acknowledgements

We thank E. Jakubikova and M. Deegbey from North Carolina State University for helpful discussions and suggestions. We also thank C. Larsen from University of Auckland for providing a useful new perspective on the Marcus analysis that we allude to in the main text and incorporated into the ESI. This work was supported in part through computational resources and services provided by the Institute for Cyber-Enabled Research at Michigan State University. The research was generously supported by the Chemical Sciences, Geosciences, and Biosciences Division, Office of Basic Energy Sciences, Office of Science, US Department of Energy under grant no. DE-FG02-01ER15282.

Author contributions

A.G. performed the transient absorption experiments and analysed the data, performed the DFT calculations and created all the figures. J.T.Y synthesized the compounds. All authors contributed to the writing of the. J.K.M directed the project.

Competing interests

The authors declare no competing interests.

Additional information

Extended data is available for this paper at https://doi.org/10.1038/s41557-024-01564-3.

Supplementary information The online version contains supplementary material available at https://doi.org/10.1038/s41557-024-01564-3.

Correspondence and requests for materials should be addressed to James K. McCusker.

Peer review information *Nature Chemistry* thanks Christopher Larsen and the other, anonymous, reviewer(s) for their contribution to the peer review of this work.

https://doi.org/10.1038/s41557-024-01564-3

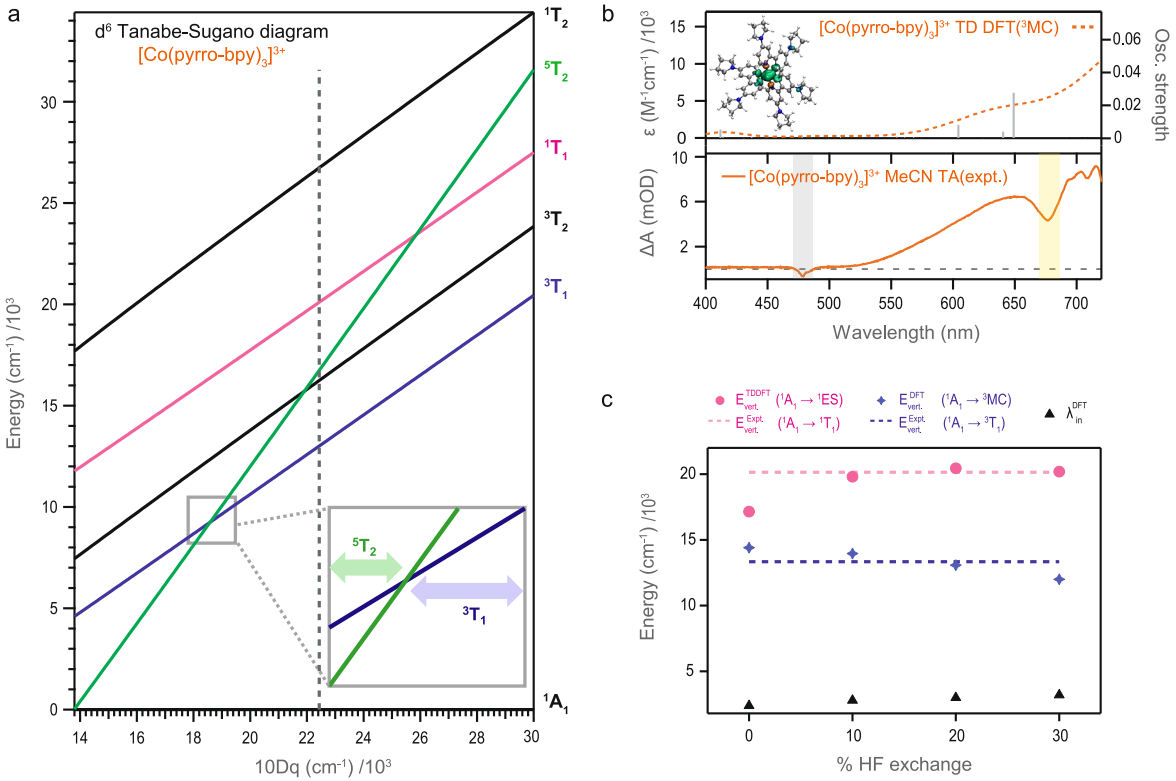

Extended Data Fig. 1 | Computational studies to estimate reorganization energy. (**a**) Tanabe-Sugano diagram appropriate for $[Co(pyrro\text{-}bpy)_3](PF_6)_3$ based on the ligand-field analysis described in ref. 29. The diagram was constructing using the experimentally determined Racah B and C parameter values of 480 cm^{-1} and 3430 cm^{-1}, respectively. The vertical dashed line corresponds to the value of 10 Dq found for $[Co(pyrro\text{-}bpy)_3](PF_6)_3$. It should be emphasized that these diagrams reflect vertical transition energies, not the zero-point energy of a given excited state that ultimately determines which state lies lowest in energy. *Inset:* An expanded view of the region near the crossing point between the $^5T_2$ and $^3T_1$ ligand-field excited states. (**b**) Comparison between time-resolved absorption spectra obtained from a singular value decomposition analysis of the experimental transient absorption data and TD-DFT-computed excited-state absorption spectra for the structurally relaxed, lowest-energy S=1 (^{3}MC) excited state. *Inset:* Spin density associated with the ^{3}MC ligand-field excited state derived from DFT calculations carried out at the optimized equilibrium geometry, showing localization of the spin density predominantly on the metal center. Positive (excess α) and negative (excess β) spin density contributions are shown as green and orange isosurfaces, respectively (isovalue = 0.003). (**c**) DFT-predicted $^1A_1 \rightarrow {}^1ES$ (pink) and $^1A_1 \rightarrow {}^3MC$ (blue) vertical transition energies compared with their experimentally determined values (dashed lines). The black triangles at the bottom of the plot correspond to the energy difference between triplet energy at singlet optimized geometry and triplet optimized geometry (black triangles) as a function of % HF exchange.